

A Well-Balanced Fifth-Order A-WENO Scheme Based on Flux Globalization

SHAOSHUAI CHU, ALEXANDER KURGANOV, AND RUIXIAO XIN

We construct a new fifth-order flux globalization based well-balanced (WB) alternative weighted essentially non-oscillatory (A-WENO) scheme for general nonconservative systems. The proposed scheme is a higher-order extension of the WB path-conservative central-upwind (PCCU) scheme recently proposed in [A. KURGANOV, Y. LIU AND R. XIN, *J. Comput. Phys.*, 474 (2023), Paper No. 111773]. We apply the new scheme to the nozzle flow system and the two-layer shallow water equations. We conduct a series of numerical experiments, which clearly demonstrate the advantages of using the fifth-order extension of the flux globalization based WB PCCU scheme.

MSC 2020 SUBJECT CLASSIFICATIONS: 65M06, 76M20, 65M08, 76M12, 35L65.

KEYWORDS AND PHRASES: A-WENO schemes, flux globalization based path-conservative central-upwind scheme, nozzle flow system, two-layer shallow water equations.

1. Introduction

This paper is focused on the development of high-order well-balanced (WB) numerical methods for the nonconservative hyperbolic systems, which in the one-dimensional (1-D) case read as

$$U_t + \mathbf{F}(U)_x = B(U)U_x. \quad (1)$$

Here, x is the spatial variable, t is time, $\mathbf{U} \in \mathbb{R}^d$ is a vector of unknowns, $\mathbf{F} : \mathbb{R}^d \rightarrow \mathbb{R}^d$ is the nonlinear flux function, and $B \in \mathbb{R}^{d \times d}$.

Developing a highly accurate numerical scheme for (1) is a challenging task due to the presence of the nonconservative product terms on the right-hand side (RHS) of the studied system, whose weak solutions can be understood as the Borel measures (see [15, 27, 28]) rather than in the sense of distributions. In addition, a good scheme for (1) should be WB, that is, it should be capable of exactly preserving some of the physically relevant

steady-state solutions of (1.1). As it was shown in [23], for many nonconservative systems steady-state solutions satisfy

$$\mathbf{F}(\mathbf{U})_x - B(\mathbf{U})\mathbf{U}_x = M(\mathbf{U})\mathbf{E}(\mathbf{U})_x = \mathbf{0}, \quad (2)$$

where $M \in \mathbb{R}^{d \times d}$ and \mathbf{E} is the vector of equilibrium variables, which are constant at the steady states.

A popular approach for developing accurate and WB numerical schemes for (1) is based on the concept of weak Borel measure solutions, which leads to a class of path-conservative schemes; see, e.g., [1, 6, 7, 8, 34, 35, 36] and references therein. One of these schemes, a second-order path-conservative central-upwind (PCCU) scheme [8], is particularly simple as it is based on Riemann-problem-solver-free central-upwind (CU) schemes, which were originally developed in [22, 24, 26] as a “black-box” solver for general multi-dimensional hyperbolic systems. One of the drawbacks of the PCCU schemes is that they can preserve simple steady states only. For instance, in the two-layer shallow water equations, the PCCU schemes can only preserve the so-called “lake-at-rest” steady states.

In [23], path-conservative techniques were incorporated into the flux globalization framework, which led to a flux globalization based WB PCCU scheme, which is capable of preserving a much wider range of steady states while still accurately treating the nonconservative products. In general, a flux globalization approach, which was introduced in [11, 5, 17, 18, 32], relies on the following quasi-conservative form of (1):

$$\mathbf{U}_t + \mathbf{K}(\mathbf{U})_x = \mathbf{0}, \quad (3)$$

where $\mathbf{K}(\mathbf{U})$ is a global flux

$$\mathbf{K}(\mathbf{U}) = \mathbf{F}(\mathbf{U}) - \mathbf{R}(\mathbf{U}), \quad \mathbf{R}(\mathbf{U}) = \int_{\hat{x}}^x [B(\mathbf{U}(\xi, t))\mathbf{U}_\xi(\xi, t)] \, d\xi, \quad (4)$$

and \hat{x} is an arbitrary number. The flux globalization based WB PCCU schemes are obtained by applying the CU numerical flux to the semi-discretization of (3) and by using the path-conservative technique to the evaluation of the integrals in (4). These schemes have been applied to a variety of hyperbolic systems in [2, 3, 4, 9, 23]. However, all of these WB PCCU schemes are only second-order accurate, which results in a limited resolution of certain complicated solution structures unless very fine mesh is used. The goal of this paper is to extend the flux globalization based WB PCCU schemes to the

fifth order of accuracy via an alternative weighted essentially non-oscillatory (A-WENO) framework.

In the past few decades, high-order finite-volume (FV) and finite-difference (FD) weighted essentially non-oscillatory (WENO) schemes have gained their popularity due to their ability to achieve high resolution. These schemes are based on high-order WENO reconstructions and interpolations; see the review papers [37, 38] and referenced therein. A drawback of FV WENO schemes is that they use FV WENO reconstructions, which are quite complicated and computationally expensive, especially in the multidimensional case. On the other hand, FD WENO schemes use 1-D WENO interpolations even in the multidimensional case, which makes them substantially simpler than their FV counterparts. The simplest and yet very accurate and powerful FD WENO schemes are A-WENO schemes were proposed in [21]; see also [10, 31, 41, 43, 42]. A-WENO schemes employ standard FV numerical fluxes (with no flux splitting required) and achieve high order of accuracy thanks to the higher-order correction terms. A-WENO schemes based on the CU numerical fluxes have been introduced in [41, 42] and extended to nonconservative systems in [13, 12].

In this paper, we develop flux globalization based WB A-WENO schemes that employ CU numerical fluxes and fifth-order path-conservative integration techniques. Our A-WENO schemes utilize new higher-order correction terms, which we have recently introduced in [14]. The designed schemes are then applied to the nozzle flow system and the two-layer shallow water equations. We perform a series of numerical experiments, which clearly demonstrate that the proposed fifth-order scheme achieves higher resolution than its second-order counterpart.

The paper is organized as follows. In §2, we give a brief overview of flux globalization based WB PCCU schemes. In §3, we construct new flux globalization based WB A-WENO schemes and then apply them to the nozzle flow system in §3.1 and the two-layer shallow water equations in §3.2. In §4, we test the new schemes on a number of challenging numerical examples. Finally, in §5, we give some concluding remarks.

2. Flux Globalization Based WB PCCU Schemes: an Overview

In this section, we give an overview of second-order flux globalization based WB PCCU schemes, which were introduced in [23] for general nonconservative systems (1) written in an equivalent quasi-conservative form (3)–(4).

We first introduce a uniform mesh consisting of the FV cells $C_j := [x_{j-\frac{1}{2}}, x_{j+\frac{1}{2}}]$ of size $x_{j+\frac{1}{2}} - x_{j-\frac{1}{2}} \equiv \Delta x$ centered at $x_j = (x_{j-\frac{1}{2}} + x_{j+\frac{1}{2}})/2$, $j = 1, \dots, N$. We assume that at a certain time level t , the approximate solution, realized in terms of the cell averages

$$\bar{U}_j(t) := \frac{1}{\Delta x} \int_{C_j} U(x, t) dx,$$

is available (in the rest of the paper, we will suppress the time-dependence of all of the indexed quantities for the sake of brevity). We then evolve the cell averages \bar{U}_j in time by solving the following system of ODEs:

$$\frac{d}{dt} \bar{U}_j = - \frac{\mathcal{K}_{j+\frac{1}{2}}^{\text{FV}} - \mathcal{K}_{j-\frac{1}{2}}^{\text{FV}}}{\Delta x}, \quad (5)$$

where $\mathcal{K}_{j+\frac{1}{2}}^{\text{FV}}$ are the WB PCCU numerical fluxes given by (see [23])

$$\mathcal{K}_{j+\frac{1}{2}}^{\text{FV}} = \frac{a_{j+\frac{1}{2}}^+ \mathbf{K}(U_{j+\frac{1}{2}}^-) - a_{j+\frac{1}{2}}^- \mathbf{K}(U_{j+\frac{1}{2}}^+)}{a_{j+\frac{1}{2}}^+ - a_{j+\frac{1}{2}}^-} + \frac{a_{j+\frac{1}{2}}^+ a_{j+\frac{1}{2}}^-}{a_{j+\frac{1}{2}}^+ - a_{j+\frac{1}{2}}^-} \left(\hat{U}_{j+\frac{1}{2}}^+ - \hat{U}_{j+\frac{1}{2}}^- \right), \quad (6)$$

$U_{j+\frac{1}{2}}^\pm$ and $\hat{U}_{j+\frac{1}{2}}^\pm$ are two slightly different approximations of the one-sided point values of $U(x_{j+\frac{1}{2}}, t)$, and $a_{j+\frac{1}{2}}^\pm$ are the one-sided local speeds of propagation, which can be estimated using the eigenvalues $\lambda_1 < \dots < \lambda_d$ of the matrix $\mathcal{A}(U) := \partial \mathbf{F} / \partial \mathbf{U} - B(U)$:

$$\begin{aligned} a_{j+\frac{1}{2}}^- &= \min \left\{ \lambda_1(\mathcal{A}(U_{j+\frac{1}{2}}^-)), \lambda_1(\mathcal{A}(U_{j+\frac{1}{2}}^+)), 0 \right\}, \\ a_{j+\frac{1}{2}}^+ &= \max \left\{ \lambda_d(\mathcal{A}(U_{j+\frac{1}{2}}^-)), \lambda_d(\mathcal{A}(U_{j+\frac{1}{2}}^+)), 0 \right\}. \end{aligned}$$

Since $\mathbf{K}(U)$ is a global flux, one needs to use a certain quadrature to evaluate its global part $\mathbf{R}(U)$. The quadrature should rely on the path-conservative technique and it also must be WB. To this end, we follow the approach introduced in [23] and compute

$$\mathbf{K}(U_{j+\frac{1}{2}}^\pm) = \mathbf{F}(U_{j+\frac{1}{2}}^\pm) - \mathbf{R}(U_{j+\frac{1}{2}}^\pm) \quad (7)$$

as follows.

First, in order to ensure the WB property of the resulting scheme, the point values $U_{j+\frac{1}{2}}^\pm$ are to be obtained with the help of a piecewise linear

reconstruction of the equilibrium variables \mathbf{E} :

$$\mathbf{E}_{j+\frac{1}{2}}^- = \mathbf{E}_j + \frac{\Delta x}{2}(\mathbf{E}_x)_j, \quad \mathbf{E}_{j+\frac{1}{2}}^+ = \mathbf{E}_{j+1} - \frac{\Delta x}{2}(\mathbf{E}_x)_{j+1}, \quad (8)$$

where $\mathbf{E}_j := \mathbf{E}(\bar{U}_j)$ and the slopes $(\mathbf{E}_x)_j$ are computed using a nonlinear limiter, for instance, the generalized minmod one (see [30, 33, 39]):

$$(\mathbf{E}_x)_j = \text{minmod} \left(\theta \frac{\mathbf{E}_{j+1} - \mathbf{E}_j}{\Delta x}, \frac{\mathbf{E}_{j+1} - \mathbf{E}_{j-1}}{2\Delta x}, \theta \frac{\mathbf{E}_j - \mathbf{E}_{j-1}}{\Delta x} \right), \quad \theta \in [1, 2],$$

applied in a component-wise manner. Here,

$$\text{minmod}(c_1, c_2, \dots) = \begin{cases} \min(c_1, c_2, \dots), & \text{if } c_i > 0, \forall i, \\ \max(c_1, c_2, \dots), & \text{if } c_i < 0, \forall i, \\ 0, & \text{otherwise.} \end{cases}$$

and the parameter θ is used to control the amount of numerical dissipation present in the resulting scheme: larger values of θ correspond to sharper but, in general, more oscillatory reconstructions. The corresponding values $\mathbf{U}_{j+\frac{1}{2}}^\pm$ are then computed by solving the (nonlinear systems of) equations

$$\mathbf{E}(\mathbf{U}_{j+\frac{1}{2}}^+) = \mathbf{E}_{j+\frac{1}{2}}^+ \quad \text{and} \quad \mathbf{E}(\mathbf{U}_{j+\frac{1}{2}}^-) = \mathbf{E}_{j+\frac{1}{2}}^- \quad (9)$$

for $\mathbf{U}_{j+\frac{1}{2}}^+$ and $\mathbf{U}_{j+\frac{1}{2}}^-$, respectively.

Equipped with $\mathbf{U}_{j+\frac{1}{2}}^\pm$, we proceed with the evaluation of $\mathbf{R}(\mathbf{U}_{j+\frac{1}{2}}^\pm)$. We select $\hat{x} = x_{\frac{1}{2}}$, set $\mathbf{R}(\mathbf{U}_{\frac{1}{2}}^-) := \mathbf{0}$, evaluate

$$\mathbf{R}(\mathbf{U}_{\frac{1}{2}}^+) = \mathbf{B}_{\Psi, \frac{1}{2}}, \quad (10)$$

and then recursively obtain

$$\mathbf{R}(\mathbf{U}_{j+\frac{1}{2}}^-) = \mathbf{R}(\mathbf{U}_{j-\frac{1}{2}}^+) + \mathbf{B}_j, \quad \mathbf{R}(\mathbf{U}_{j+\frac{1}{2}}^+) = \mathbf{R}(\mathbf{U}_{j+\frac{1}{2}}^-) + \mathbf{B}_{\Psi, j+\frac{1}{2}}, \quad (11)$$

for $j = 1, \dots, N$. In (10) and (11), $\mathbf{B}_{\Psi, j+\frac{1}{2}}$ and \mathbf{B}_j are obtained using a proper quadrature for the integrals in

$$\mathbf{B}_{\Psi, j+\frac{1}{2}} = \int_0^1 B(\Psi_{j+\frac{1}{2}}(s)) \Psi'_{j+\frac{1}{2}}(s) ds, \quad \mathbf{B}_j = \int_{C_j} B(\mathbf{U}) \mathbf{U}_x dx,$$

where $\Psi_{j+\frac{1}{2}}(s) = \Psi_{j+\frac{1}{2}}(s; \mathbf{U}_{j+\frac{1}{2}}^-, \mathbf{U}_{j+\frac{1}{2}}^+)$ is a sufficiently smooth path connecting the states $\mathbf{U}_{j+\frac{1}{2}}^-$ and $\mathbf{U}_{j+\frac{1}{2}}^+$, that is,

$$\begin{aligned} \Psi_{j+\frac{1}{2}} &: [0, 1] \times \mathbb{R}^d \times \mathbb{R}^d \rightarrow \mathbb{R}^d, \\ \Psi_{j+\frac{1}{2}}(0; \mathbf{U}_{j+\frac{1}{2}}^-, \mathbf{U}_{j+\frac{1}{2}}^+) &= \mathbf{U}_{j+\frac{1}{2}}^-, \quad \Psi_{j+\frac{1}{2}}(1; \mathbf{U}_{j+\frac{1}{2}}^-, \mathbf{U}_{j+\frac{1}{2}}^+) = \mathbf{U}_{j+\frac{1}{2}}^+. \end{aligned}$$

In order to ensure the resulting scheme to be WB, one has to connect the left and right equilibrium states $\mathbf{E}_{j+\frac{1}{2}}^-$ and $\mathbf{E}_{j+\frac{1}{2}}^+$. We use a linear segment path

$$\mathbf{E}_{j+\frac{1}{2}}(s) = \mathbf{E}_{j+\frac{1}{2}}^- + s(\mathbf{E}_{j+\frac{1}{2}}^+ - \mathbf{E}_{j+\frac{1}{2}}^-), \quad s \in [0, 1],$$

which is then used together with (2) and trapezoidal quadrature to end up with

$$\mathbf{B}_{\Psi, j+\frac{1}{2}} = \mathbf{F}_{j+\frac{1}{2}}^+ - \mathbf{F}_{j+\frac{1}{2}}^- - \frac{1}{2} \left[M(\mathbf{U}_{j+\frac{1}{2}}^+) + M(\mathbf{U}_{j+\frac{1}{2}}^-) \right] (\mathbf{E}_{j+\frac{1}{2}}^+ - \mathbf{E}_{j+\frac{1}{2}}^-).$$

For \mathbf{B}_j , we similarly have

$$\begin{aligned} \mathbf{B}_j &= \mathbf{F}(\mathbf{U}_{j+\frac{1}{2}}^-) - \mathbf{F}(\mathbf{U}_{j-\frac{1}{2}}^+) - \int_{C_j} M(\mathbf{U}) \mathbf{E}(\mathbf{U})_x dx \\ &\approx \mathbf{F}(\mathbf{U}_{j+\frac{1}{2}}^-) - \mathbf{F}(\mathbf{U}_{j-\frac{1}{2}}^+) - \frac{1}{2} \left[M(\mathbf{U}_{j+\frac{1}{2}}^-) + M(\mathbf{U}_{j-\frac{1}{2}}^+) \right] (\mathbf{E}_{j+\frac{1}{2}}^- - \mathbf{E}_{j-\frac{1}{2}}^+). \end{aligned} \tag{12}$$

Finally, in (6), $\widehat{\mathbf{U}}_{j+\frac{1}{2}}^\pm$ are obtained by solving modified versions of (9):

$$\widehat{\mathbf{E}}(\widehat{\mathbf{U}}_{j+\frac{1}{2}}^+) = \mathbf{E}_{j+\frac{1}{2}}^+ \quad \text{and} \quad \widehat{\mathbf{E}}(\widehat{\mathbf{U}}_{j+\frac{1}{2}}^-) = \mathbf{E}_{j+\frac{1}{2}}^-.$$

Here, the functions $\widehat{\mathbf{E}}$ are the modifications of the functions \mathbf{E} , which are made in such a way that $\widehat{\mathbf{U}}_{j+\frac{1}{2}}^+ = \widehat{\mathbf{U}}_{j+\frac{1}{2}}^-$ as long as $\widehat{\mathbf{E}}_{j+\frac{1}{2}}^+ = \widehat{\mathbf{E}}_{j+\frac{1}{2}}^-$ and, at the same time, $\widehat{\mathbf{U}}_{j+\frac{1}{2}}^+ = \mathbf{U}_{j+\frac{1}{2}}^+ + \mathcal{O}((\Delta x)^2)$ and $\widehat{\mathbf{U}}_{j+\frac{1}{2}}^- = \mathbf{U}_{j+\frac{1}{2}}^- + \mathcal{O}((\Delta x)^2)$ for smooth solutions.

3. Flux Globalization Based WB A-WENO Schemes

In this section, we extend the second-order WB PCCU schemes from §2 to the fifth order of accuracy via the A-WENO framework:

$$\frac{d\mathbf{U}_j}{dt} = -\frac{\mathcal{K}_{j+\frac{1}{2}} - \mathcal{K}_{j-\frac{1}{2}}}{\Delta x}, \tag{13}$$

where $\mathbf{U}_j \approx \mathbf{U}(x_j, t)$ and $\mathcal{K}_{j+\frac{1}{2}}$ are the fifth-order A-WENO numerical fluxes:

$$\mathcal{K}_{j+\frac{1}{2}} = \mathcal{K}_{j+\frac{1}{2}}^{\text{FV}} - \frac{(\Delta x)^2}{24} (\mathbf{K}_{xx})_{j+\frac{1}{2}} + \frac{7(\Delta x)^4}{5760} (\mathbf{K}_{xxxx})_{j+\frac{1}{2}}.$$

Here, $\mathcal{K}_{j+\frac{1}{2}}^{\text{FV}}$ is the WB PCCU numerical flux introduced in §2, and the higher-order correction terms $(\mathbf{K}_{xx})_{j+\frac{1}{2}}$ and $(\mathbf{K}_{xxxx})_{j+\frac{1}{2}}$ are FD approximations of the second- and fourth-order spatial derivatives of \mathbf{K} at $x = x_{j+\frac{1}{2}}$, respectively. We follow [14] and compute the correction terms using the numerical fluxes, which have been already obtained:

$$\begin{aligned} (\mathbf{K}_{xx})_{j+\frac{1}{2}} &= \frac{1}{12(\Delta x)^2} \left[-\mathcal{K}_{j-\frac{3}{2}}^{\text{FV}} + 16\mathcal{K}_{j-\frac{1}{2}}^{\text{FV}} - 30\mathcal{K}_{j+\frac{1}{2}}^{\text{FV}} + 16\mathcal{K}_{j+\frac{3}{2}}^{\text{FV}} - \mathcal{K}_{j+\frac{5}{2}}^{\text{FV}} \right], \\ (\mathbf{K}_{xxxx})_{j+\frac{1}{2}} &= \frac{1}{(\Delta x)^4} \left[\mathcal{K}_{j-\frac{3}{2}}^{\text{FV}} - 4\mathcal{K}_{j-\frac{1}{2}}^{\text{FV}} + 6\mathcal{K}_{j+\frac{1}{2}}^{\text{FV}} - 4\mathcal{K}_{j+\frac{3}{2}}^{\text{FV}} + \mathcal{K}_{j+\frac{5}{2}}^{\text{FV}} \right]. \end{aligned}$$

Finally, in order the resulting scheme to be fifth-order accurate, we apply the fifth-order affine-invariant WENO-Z (Ai-WENO-Z) interpolation [16, 40, 29] to evaluate $\mathbf{E}_{j+\frac{1}{2}}^{\pm}$ (instead of the piecewise linear reconstruction (8)). In addition, the integral in (12) needs to be evaluated using a quadrature, which is at least fifth-order accurate. In this paper, we use the Newton-Cotes quadrature introduced in [13, (4.4)].

3.1. Application to the Nozzle Flow System

In this section, we apply the flux globalization based WB A-WENO scheme to the nozzle flow system, which reads as (1) with

$$\mathbf{U} = \begin{pmatrix} \sigma\rho \\ \sigma\rho u \\ \sigma \end{pmatrix}, \quad \mathbf{F}(\mathbf{U}) = \begin{pmatrix} \sigma\rho u \\ \sigma\rho u^2 + \sigma p \\ 0 \end{pmatrix}, \quad B(\mathbf{U}) = \begin{pmatrix} 0 & 0 & 0 \\ 0 & 0 & p \\ 0 & 0 & 0 \end{pmatrix}, \quad (14)$$

where $p(\rho) = \kappa\rho^\gamma$, and admits steady-state solutions satisfying (2) with

$$M(\mathbf{U}) := \begin{pmatrix} 1 & 0 & 0 \\ u & \sigma\rho & 0 \\ 0 & 0 & 1 \end{pmatrix}, \quad \mathbf{E}(\mathbf{U}) = \begin{pmatrix} q \\ E \\ 0 \end{pmatrix},$$

$$q := \sigma\rho u, \quad E := \frac{u^2}{2} + \frac{\kappa\gamma}{\gamma-1}\rho^{\gamma-1}.$$

Here, ρ is the density, u is the velocity, p is the pressure, $\kappa > 0$ and $1 < \gamma < \frac{5}{3}$ are constants, and $\sigma = \sigma(x)$ denotes the cross-section of the nozzle, which is a given function independent of time. The nozzle flow system (1), (14) can be rewritten in the quasi-conservative form (3)–(4) with

$$\mathbf{K}(\mathbf{U}) = \begin{pmatrix} \sigma\rho u \\ K \\ 0 \end{pmatrix}, \quad \mathbf{R}(\mathbf{U}) = \begin{pmatrix} 0 \\ R \\ 0 \end{pmatrix}, \quad (15)$$

where

$$K = \sigma\rho u^2 + \sigma p - R, \quad R := \int_{\hat{x}}^x p(\xi, t) \sigma_\xi(\xi) d\xi.$$

In order to construct the fifth-order WB A-WENO scheme, we first compute

$$E_j = \frac{u_j^2}{2} + \frac{\kappa\gamma}{\gamma-1}(\rho_j)^{\gamma-1},$$

where $u_j := \bar{q}_j / (\overline{\sigma\rho})_j$, $\rho_j := \overline{(\sigma\rho)}_j / \sigma_j$, and $\sigma_j := \sigma(x_j)$. Given \bar{q}_j and E_j , we perform the Ai-WENO-Z interpolation to obtain the point values $q_{j+\frac{1}{2}}^\pm$ and $E_{j+\frac{1}{2}}^\pm$, and then numerically solve the nonlinear equations

$$E_{j+\frac{1}{2}}^\pm = \frac{(q_{j+\frac{1}{2}}^\pm)^2}{2((\sigma\rho)_{j+\frac{1}{2}}^\pm)^2} + \frac{\kappa\gamma}{\gamma-1}(\sigma_{j+\frac{1}{2}}^\pm)^{1-\gamma} [(\sigma\rho)_{j+\frac{1}{2}}^\pm]^{\gamma-1}$$

for $(\sigma\rho)_{j+\frac{1}{2}}^\pm$. Here, the values $\sigma_{j+\frac{1}{2}}^\pm$ are obtained by a Ai-WENO-Z interpolation of σ . For solution details, see [23].

After obtaining the values $(\sigma\rho)_{j+\frac{1}{2}}^\pm$, we compute the corresponding values $u_{j+\frac{1}{2}}^\pm = q_{j+\frac{1}{2}}^\pm/(\sigma\rho)_{j+\frac{1}{2}}^\pm$ and $\rho_{j+\frac{1}{2}}^\pm = (\sigma\rho)_{j+\frac{1}{2}}^\pm/\sigma_{j+\frac{1}{2}}^\pm$, which are then used to estimate the one-sided local speeds of propagation:

$$\begin{aligned} a_{j+\frac{1}{2}}^+ &= \max \left\{ u_{j+\frac{1}{2}}^+ + \sqrt{\kappa\gamma} (\rho_{j+\frac{1}{2}}^+)^{\frac{\gamma-1}{2}}, u_{j+\frac{1}{2}}^- + \sqrt{\kappa\gamma} (\rho_{j+\frac{1}{2}}^-)^{\frac{\gamma-1}{2}}, 0 \right\}, \\ a_{j+\frac{1}{2}}^- &= \min \left\{ u_{j+\frac{1}{2}}^+ - \sqrt{\kappa\gamma} (\rho_{j+\frac{1}{2}}^+)^{\frac{\gamma-1}{2}}, u_{j+\frac{1}{2}}^- - \sqrt{\kappa\gamma} (\rho_{j+\frac{1}{2}}^-)^{\frac{\gamma-1}{2}}, 0 \right\}. \end{aligned}$$

The global flux \mathbf{K} in (15) needs to be evaluated by (7), which for the nozzle flow system reads as

$$\mathbf{K}(\mathbf{U}_{j+\frac{1}{2}}^\pm) = \mathbf{F}(\mathbf{U}_{j+\frac{1}{2}}^\pm) - \mathbf{R}(\mathbf{U}_{j+\frac{1}{2}}^\pm) = \begin{pmatrix} q_{j+\frac{1}{2}}^\pm \\ q_{j+\frac{1}{2}}^\pm u_{j+\frac{1}{2}}^\pm + \sigma_{j+\frac{1}{2}}^\pm p_{j+\frac{1}{2}}^\pm \\ 0 \end{pmatrix} - \begin{pmatrix} 0 \\ R_{j+\frac{1}{2}}^\pm \\ 0 \end{pmatrix},$$

where $p_{j+\frac{1}{2}}^\pm = \kappa(\rho_{j+\frac{1}{2}}^\pm)^\gamma$ and $R_{j+\frac{1}{2}}^\pm$ are computed as in §2. In particular, we have $R_{\frac{1}{2}}^- := 0$, $R_{\frac{1}{2}}^+ = B_{\Psi, \frac{1}{2}}$, and

$$R_{j+\frac{1}{2}}^- = R_{j-\frac{1}{2}}^+ + B_j, \quad R_{j+\frac{1}{2}}^+ = R_{j+\frac{1}{2}}^- + B_{\Psi, j+\frac{1}{2}}, \quad j = 1, \dots, N,$$

where

$$\begin{aligned} B_{\Psi, j+\frac{1}{2}} &= q_{j+\frac{1}{2}}^+ u_{j+\frac{1}{2}}^+ + \sigma_{j+\frac{1}{2}}^+ p_{j+\frac{1}{2}}^+ - q_{j+\frac{1}{2}}^- u_{j+\frac{1}{2}}^- - \sigma_{j+\frac{1}{2}}^- p_{j+\frac{1}{2}}^- \\ &\quad - \frac{u_{j+\frac{1}{2}}^+ + u_{j+\frac{1}{2}}^-}{2} (q_{j+\frac{1}{2}}^+ - q_{j+\frac{1}{2}}^-) - \frac{(\sigma\rho)_{j+\frac{1}{2}}^+ + (\sigma\rho)_{j+\frac{1}{2}}^-}{2} (E_{j+\frac{1}{2}}^+ - E_{j+\frac{1}{2}}^-), \end{aligned}$$

and

$$B_j = q_{j+\frac{1}{2}}^- u_{j+\frac{1}{2}}^- + \sigma_{j+\frac{1}{2}}^- p_{j+\frac{1}{2}}^- - q_{j-\frac{1}{2}}^+ u_{j-\frac{1}{2}}^+ - \sigma_{j-\frac{1}{2}}^+ p_{j-\frac{1}{2}}^+ - \int_{C_j} (uq_x + \sigma\rho E_x) dx,$$

where the integral in the last formula is evaluated using the fifth-order Newton-Cotes quadrature [13, (4.4)].

Finally, $\widehat{\mathbf{U}}_{j+\frac{1}{2}}^\pm := ((\widehat{\sigma\rho})_{j+\frac{1}{2}}^\pm, \widehat{q}_{j+\frac{1}{2}}^\pm)^\top$, where $\widehat{q}_{j+\frac{1}{2}}^\pm = q_{j+\frac{1}{2}}^\pm$ and $(\widehat{\sigma\rho})_{j+\frac{1}{2}}^\pm$ are obtained by numerically solving the following nonlinear equations:

$$E_{j+\frac{1}{2}}^\pm = \frac{(q_{j+\frac{1}{2}}^\pm)^2}{2((\widehat{\sigma\rho})_{j+\frac{1}{2}}^\pm)^2} + \frac{\kappa\gamma}{\gamma-1} (\widehat{\sigma}_{j+\frac{1}{2}}^\pm)^{1-\gamma} [(\widehat{\sigma\rho})_{j+\frac{1}{2}}^\pm]^{\gamma-1}$$

with $\widehat{\sigma}_{j+\frac{1}{2}} := (\sigma_{j+\frac{1}{2}}^+ + \sigma_{j+\frac{1}{2}}^-)/2$; for solution details, see [23].

3.2. Application to the Two-Layer Shallow Water Equations

In this section, we apply the flux globalization based WB A-WENO scheme to the two-layer shallow water equations, which read as (1) with

$$\begin{aligned} \mathbf{U} &= \begin{pmatrix} h_1 \\ q_1 \\ h_2 \\ q_2 \\ Z \end{pmatrix}, \quad \mathbf{F}(\mathbf{U}) = \begin{pmatrix} q_1 \\ h_1 u_1^2 + \frac{g}{2} h_1^2 \\ q_2 \\ h_2 u_2^2 + \frac{g}{2} h_2^2 \\ 0 \end{pmatrix}, \\ B(\mathbf{U}) &= \begin{pmatrix} 0 & 0 & 0 & 0 & 0 \\ 0 & 0 & -gh_1 & 0 & -gh_1 \\ 0 & 0 & 0 & 0 & 0 \\ -rgh_2 & 0 & 0 & 0 & -gh_2 \\ 0 & 0 & 0 & 0 & 0 \end{pmatrix}, \end{aligned} \tag{16}$$

and admit steady-state solutions satisfying (2) with

$$M(\mathbf{U}) := \begin{pmatrix} 1 & 0 & 0 & 0 & 0 \\ u_1 & h_1 & 0 & 0 & 0 \\ 0 & 0 & 1 & 0 & 0 \\ 0 & 0 & u_2 & h_2 & 0 \\ 0 & 0 & 0 & 0 & 1 \end{pmatrix}, \quad \mathbf{E}(\mathbf{U}) := \begin{pmatrix} q_1 \\ E_1 \\ q_2 \\ E_2 \\ 0 \end{pmatrix},$$

where

$$E_1 := \frac{q_1^2}{2h_1^2} + g(h_1 + h_2 + Z) \quad \text{and} \quad E_2 := \frac{q_2^2}{2h_2^2} + g(rh_1 + h_2 + Z).$$

Here, h_1 and h_2 are the water depths in the upper and lower layers, respectively, u_1 and u_2 are the corresponding velocities, $q_1 := h_1 u_1$ and $q_2 := h_2 u_2$ represent the corresponding discharges, $Z(x)$ is a function describing the bottom topography, which can be discontinuous, g is the constant acceleration due to gravity, and $r := \frac{\rho_1}{\rho_2} < 1$ is the ratio of the constant densities ρ_1

(upper layer) and ρ_2 (lower layer). The two-layer shallow water equations (1), (16) can be rewritten in the quasi-conservative form (3)–(4) with

$$\mathbf{K}(\mathbf{U}) = (q_1, K_1, q_2, K_2, 0)^\top, \quad \mathbf{R}(\mathbf{U}) = (0, R_1, 0, R_2, 0)^\top,$$

where

$$\begin{aligned} K_1 &= h_1 u_1^2 + \frac{g}{2} h_1^2 - R_1, & R_1 &:= - \int_{\hat{x}}^x g h_1(\xi, t) [h_2(\xi, t) + Z(\xi)]_\xi d\xi, \\ K_2 &= h_2 u_2^2 + \frac{g}{2} h_2^2 - R_2, & R_2 &:= - \int_{\hat{x}}^x g h_2(\xi, t) [r h_1(\xi, t) + Z(\xi)]_\xi d\xi. \end{aligned} \quad (17)$$

In order to construct the fifth-order WB A-WENO scheme, we first compute

$$\begin{aligned} (E_1)_j &:= \frac{(\bar{q}_1)_j^2}{2(\bar{h}_1)_j^2} + g [(\bar{h}_1)_j + (\bar{h}_2)_j + Z_j], \\ (E_2)_j &:= \frac{(\bar{q}_2)_j^2}{2(\bar{h}_2)_j^2} + g [r(\bar{h}_1)_j + (\bar{h}_2)_j + Z_j], \end{aligned}$$

where $Z_j := Z(x_j)$. Given $(\bar{q}_1)_j$, $(\bar{q}_2)_j$, $(E_1)_j$, and $(E_2)_j$, we perform the Ai-WENO-Z interpolation to obtain the point values $\mathbf{E}_{j+\frac{1}{2}}^\pm = ((q_1)_{j+\frac{1}{2}}^\pm, (E_1)_{j+\frac{1}{2}}^\pm, (q_2)_{j+\frac{1}{2}}^\pm, (E_2)_{j+\frac{1}{2}}^\pm, 0)^\top$, and then at every cell interfaces $x = x_{j+\frac{1}{2}}$, we numerically solve the (nonlinear) systems of equations

$$\begin{cases} (E_1)_{j+\frac{1}{2}}^+ = \frac{((q_1)_{j+\frac{1}{2}}^+)^2}{2((h_1)_{j+\frac{1}{2}}^+)^2} + g [(h_1)_{j+\frac{1}{2}}^+ + (h_2)_{j+\frac{1}{2}}^+ + Z_{j+\frac{1}{2}}^+], \\ (E_2)_{j+\frac{1}{2}}^+ = \frac{((q_2)_{j+\frac{1}{2}}^+)^2}{2((h_2)_{j+\frac{1}{2}}^+)^2} + g [r(h_1)_{j+\frac{1}{2}}^+ + (h_2)_{j+\frac{1}{2}}^+ + Z_{j+\frac{1}{2}}^+], \end{cases} \quad (18)$$

and

$$\begin{cases} (E_1)_{j+\frac{1}{2}}^- = \frac{((q_1)_{j+\frac{1}{2}}^-)^2}{2((h_1)_{j+\frac{1}{2}}^-)^2} + g \left[(h_1)_{j+\frac{1}{2}}^- + (h_2)_{j+\frac{1}{2}}^- + Z_{j+\frac{1}{2}}^- \right], \\ (E_2)_{j+\frac{1}{2}}^- = \frac{((q_2)_{j+\frac{1}{2}}^-)^2}{2((h_2)_{j+\frac{1}{2}}^-)^2} + g \left[r(h_1)_{j+\frac{1}{2}}^- + (h_2)_{j+\frac{1}{2}}^- + Z_{j+\frac{1}{2}}^- \right], \end{cases} \quad (19)$$

for $((h_1)_{j+\frac{1}{2}}^+, (h_2)_{j+\frac{1}{2}}^+)$ and $((h_1)_{j+\frac{1}{2}}^-, (h_2)_{j+\frac{1}{2}}^-)$, respectively. Here, the values $Z_{j+\frac{1}{2}}^\pm$ in (18) and (19) are obtained using the Ai-WENO-Z interpolation of Z . For solution details, see [23].

After obtaining the values $(h_1)_{j+\frac{1}{2}}^\pm$ and $(h_2)_{j+\frac{1}{2}}^\pm$, we compute the corresponding values $(u_i)_{j+\frac{1}{2}}^\pm = (q_i)_{j+\frac{1}{2}}^\pm / (h_i)_{j+\frac{1}{2}}^\pm$, $i = 1, 2$, and then evaluate the global numerical fluxes $\mathbf{K}(\mathbf{U}_{j+\frac{1}{2}}^\pm)$ at the cell interfaces $x = x_{j+\frac{1}{2}}$ using (16)–(17):

$$\begin{aligned} \mathbf{K}(\mathbf{U}_{j+\frac{1}{2}}^\pm) &= \mathbf{F}(\mathbf{U}_{j+\frac{1}{2}}^\pm) - \mathbf{R}(\mathbf{U}_{j+\frac{1}{2}}^\pm) \\ &= \begin{pmatrix} (q_1)_{j+\frac{1}{2}}^\pm \\ (h_1)_{j+\frac{1}{2}}^\pm \left((u_1)_{j+\frac{1}{2}}^\pm \right)^2 + \frac{g}{2} \left((h_1)_{j+\frac{1}{2}}^\pm \right)^2 \\ (q_2)_{j+\frac{1}{2}}^\pm \\ (h_2)_{j+\frac{1}{2}}^\pm \left((u_2)_{j+\frac{1}{2}}^\pm \right)^2 + \frac{g}{2} \left((h_2)_{j+\frac{1}{2}}^\pm \right)^2 \\ 0 \end{pmatrix} - \begin{pmatrix} 0 \\ (R_1)_{j+\frac{1}{2}}^\pm \\ 0 \\ (R_2)_{j+\frac{1}{2}}^\pm \\ 0 \end{pmatrix}, \end{aligned}$$

where $(R_i)_{j+\frac{1}{2}}^\pm$, $i = 1, 2$ are computed as in §2. In particular, we have $(R_i)_{\frac{1}{2}}^- := 0$, $(R_i)_{\frac{1}{2}}^+ = (B_i)_{\Psi, \frac{1}{2}}$, and

$$(R_i)_{j+\frac{1}{2}}^- = (R_i)_{j-\frac{1}{2}}^+ + (B_i)_j, \quad (R_i)_{j+\frac{1}{2}}^+ = (R_i)_{j+\frac{1}{2}}^- + (B_i)_{\Psi, j+\frac{1}{2}}, \quad j = 1, \dots, N,$$

where

$$\begin{aligned} (B_i)_{\Psi, j+\frac{1}{2}} &= (q_i)_{j+\frac{1}{2}}^+ (u_i)_{j+\frac{1}{2}}^+ - (q_i)_{j+\frac{1}{2}}^- (u_i)_{j+\frac{1}{2}}^- + \frac{g}{2} \left[((h_i)_{j+\frac{1}{2}}^+)^2 - ((h_i)_{j+\frac{1}{2}}^-)^2 \right] \\ &\quad - \frac{(u_i)_{j+\frac{1}{2}}^+ + (u_i)_{j+\frac{1}{2}}^-}{2} \left[(q_i)_{j+\frac{1}{2}}^+ - (q_i)_{j+\frac{1}{2}}^- \right] \\ &\quad - \frac{(h_i)_{j+\frac{1}{2}}^+ + (h_i)_{j+\frac{1}{2}}^-}{2} \left[(E_i)_{j+\frac{1}{2}}^+ - (E_i)_{j+\frac{1}{2}}^- \right], \end{aligned}$$

and

$$\begin{aligned} (B_i)_j &= (q_i)_{j+\frac{1}{2}}^- (u_i)_{j+\frac{1}{2}}^- - (q_i)_{j-\frac{1}{2}}^+ (u_i)_{j-\frac{1}{2}}^+ + \frac{g}{2} \left[((h_i)_{j+\frac{1}{2}}^-)^2 - ((h_i)_{j-\frac{1}{2}}^+)^2 \right] \\ &\quad - \int_{C_j} (u_i (q_i)_x + h_i (E_i)_x) dx, \end{aligned}$$

$i = 1, 2$. As in §3.1, the integral in the last formula is evaluated using the fifth-order Newton-Cotes quadrature [13, (4.4)]. The one-sided local speed $a_{j+\frac{1}{2}}^\pm$ are estimated using the Lagrange theorem precisely as it was done in [25, §2.3].

Finally, $\widehat{\mathbf{U}}_{j+\frac{1}{2}}^\pm := ((\widehat{h}_1)_{j+\frac{1}{2}}^\pm, (\widehat{q}_1)_{j+\frac{1}{2}}^\pm, (\widehat{h}_2)_{j+\frac{1}{2}}^\pm, (\widehat{q}_2)_{j+\frac{1}{2}}^\pm)^\top$, where $(\widehat{q}_i)_{j+\frac{1}{2}}^\pm = (q_i)_{j+\frac{1}{2}}^\pm$, $i = 1, 2$, and $(\widehat{h}_i)_{j+\frac{1}{2}}^\pm$, $i = 1, 2$, are obtained by numerically solving the following (nonlinear) systems:

$$\begin{cases} (E_1)_{j+\frac{1}{2}}^+ = \frac{((q_1)_{j+\frac{1}{2}}^+)^2}{2((\widehat{h}_1)_{j+\frac{1}{2}}^+)^2} + g \left[(\widehat{h}_1)_{j+\frac{1}{2}}^+ + (\widehat{h}_2)_{j+\frac{1}{2}}^+ + \widehat{Z}_{j+\frac{1}{2}} \right], \\ (E_2)_{j+\frac{1}{2}}^+ = \frac{((q_2)_{j+\frac{1}{2}}^+)^2}{2((\widehat{h}_2)_{j+\frac{1}{2}}^+)^2} + g \left[r(\widehat{h}_1)_{j+\frac{1}{2}}^+ + (\widehat{h}_2)_{j+\frac{1}{2}}^+ + \widehat{Z}_{j+\frac{1}{2}} \right], \end{cases}$$

and

$$\begin{cases} (E_1)_{j+\frac{1}{2}}^- = \frac{((q_1)_{j+\frac{1}{2}}^-)^2}{2((\widehat{h}_1)_{j+\frac{1}{2}}^-)^2} + g \left[(\widehat{h}_1)_{j+\frac{1}{2}}^- + (\widehat{h}_2)_{j+\frac{1}{2}}^- + \widehat{Z}_{j+\frac{1}{2}} \right], \\ (E_2)_{j+\frac{1}{2}}^- = \frac{((q_2)_{j+\frac{1}{2}}^-)^2}{2((\widehat{h}_2)_{j+\frac{1}{2}}^-)^2} + g \left[r(\widehat{h}_1)_{j+\frac{1}{2}}^- + (\widehat{h}_2)_{j+\frac{1}{2}}^- + \widehat{Z}_{j+\frac{1}{2}} \right], \end{cases}$$

with $\widehat{Z}_{j+\frac{1}{2}} := (Z_{j+\frac{1}{2}}^+ + Z_{j+\frac{1}{2}}^-)/2$; for solution details, see [23].

4. Numerical Examples

In this section, we apply the developed fifth-order WB A-WENO schemes to several numerical examples taken from [23] and compare their performance with that of the corresponding second-order schemes. For the sake of brevity, the tested schemes will be referred to as the 5-Order Scheme and 2-Order Scheme, respectively.

In all of the examples, we have solved the ODE systems (5) and (13) using the three-stage third-order strong stability preserving (SSP) Runge-Kutta solver (see, e.g., [19, 20]) and use the CFL number 0.5. The 2-Order Scheme has been implemented with the minmod parameter $\theta = 1.3$.

4.1. Nozzle Flow System

We begin with two examples for the nozzle flow system (1), (14) with $\kappa = 1$ and $\gamma = 1.4$. In both examples, we consider nontrivial steady states, which can be exactly preserved by both 2-Order and 5-Order Schemes at discrete level (this has been numerically verified), and test the ability of the studied schemes to capture small perturbations of these steady states.

Example 1—Flows in Continuous Convergent and Divergent Nozzles. In the first example, we consider convergent and divergent nozzles described using the smooth cross-sections

$$\sigma(x) = 0.976 - 0.748 \tanh(0.8x - 4) \quad \text{and} \quad \sigma(x) = 0.976 + 0.748 \tanh(0.8x - 4),$$

respectively.

We take the steady states with $q_{\text{eq}} \equiv 8$, $E_{\text{eq}} = 58.3367745090349$ and $q_{\text{eq}} = 8$, $E_{\text{eq}} = 21.9230562619897$ for the convergent and divergent nozzles, respectively, and compute the discrete values of $\rho_{\text{eq}}(x)$ in both the convergent and divergent cases by solving the corresponding nonlinear equations. We then obtain $u_{\text{eq}}(x) = q_{\text{eq}}(x)/(\sigma(x)\rho_{\text{eq}}(x))$.

Equipped with these steady states, we proceed by adding a small perturbation to the density field and consider the initial data

$$\rho(x, 0) = \rho_{\text{eq}}(x) + \begin{cases} 10^{-2}, & x \in [2.9, 3.1], \\ 0, & \text{otherwise,} \end{cases} \quad q(x, 0) = \sigma(x)\rho(x, 0)u_{\text{eq}}(x),$$

prescribed in the computational domain $[0, 10]$ subject to free boundary conditions.

We compute the numerical solutions until the final time $t = 0.5$ by both the 2-Order and 5-Order Schemes for both convergent and divergent nozzles on a uniform mesh with $\Delta x = 1/20$ and plot the differences $\rho(x, t) - \rho_{\text{eq}}(x)$ at times $t = 0.1, 0.3,$ and 0.5 in Figures 1 and 2. We also plot the reference solutions computed by the 5-Order Scheme with $\Delta x = 1/400$. As one can see, the 5-Order Scheme clearly outperforms the 2-Order Scheme as it achieves much higher resolution of the perturbations.

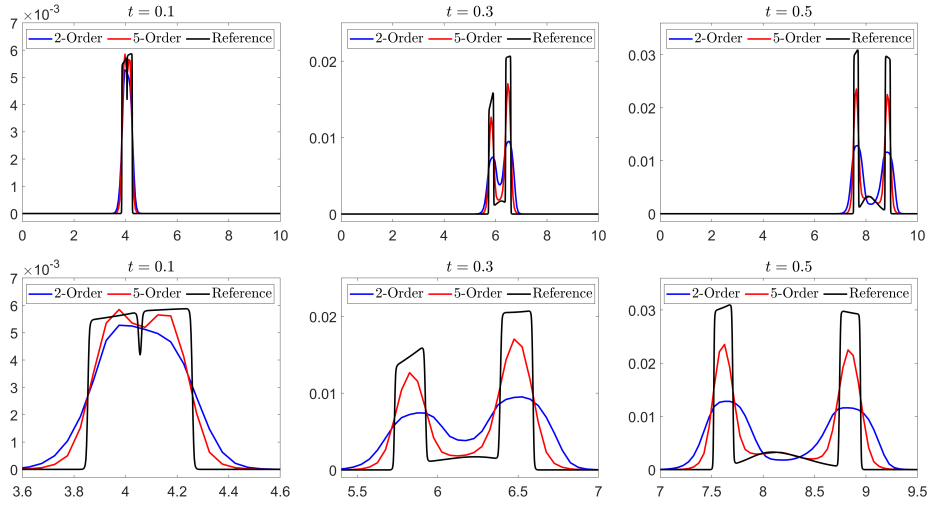


Figure 1: Example 1 (Convergent Nozzle): The difference $\rho(x, t) - \rho_{\text{eq}}$ (top row) and zoom at the perturbations (bottom row) at times $t = 0.1$ (left column), 0.3 (middle column), and 0.5 (right column).

Example 2—Flows in a Discontinuous Convergent-Divergent Nozzle. In the second example, we consider a convergent-divergent nozzle with a discontinuous $\sigma(x)$ given by

$$\sigma(x) = \begin{cases} 2, & x \in [0, 7.5] \cup [12.5, 20], \\ 1, & \text{otherwise.} \end{cases}$$

We take a steady state with $q_{\text{eq}} \equiv 8$ and $E_{\text{eq}} = 57.13486505$ and compute the discrete values of $\rho_{\text{eq}}(x)$ by solving the corresponding nonlinear equations. We then obtain $u_{\text{eq}}(x) = q_{\text{eq}}(x)/(\sigma(x)\rho_{\text{eq}}(x))$.

Equipped with these steady states, we proceed by adding a small per-

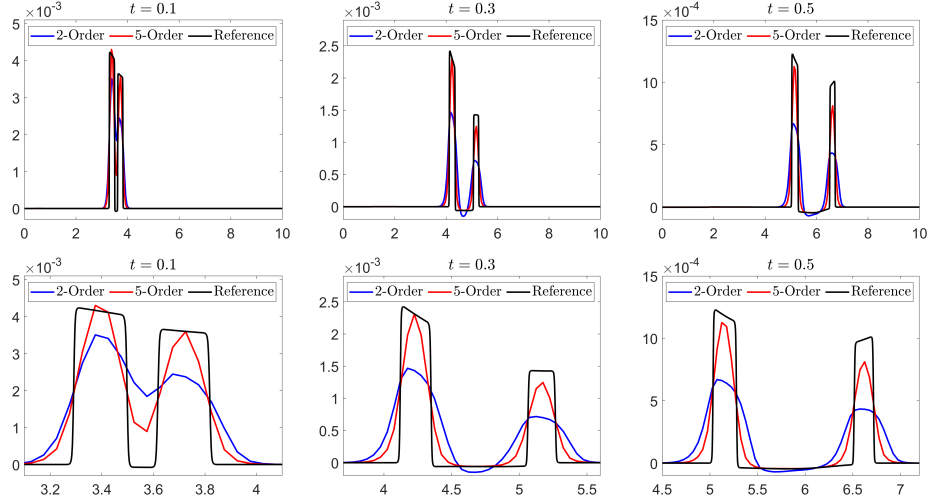


Figure 2: Example 1: Same as in Figure 1, but for the divergent nozzle.

turbation to the density field and consider the initial data

$$\rho(x, 0) = \rho_{\text{eq}}(x) + \begin{cases} 10^{-2}, & x \in [1, 2], \\ 0, & \text{otherwise,} \end{cases} \quad q(x, 0) = \sigma(x)\rho(x, 0)u_{\text{eq}}(x),$$

prescribed in the computational domain $[0, 20]$ subject to free boundary conditions.

We compute the solutions until the final time $t = 1$ by both the 2-Order and 5-Order Schemes on a uniform mesh with $\Delta x = 1/10$. In Figure 3, we plot the difference $\rho(x, t) - \rho_{\text{eq}}(x)$ at times $t = 0.2, 0.6$, and 1 together the reference solutions computed by the 5-Order Scheme with $\Delta x = 1/100$. The obtained results clearly demonstrate that the 5-Order Scheme achieves higher resolution than the 2-Order Scheme, especially at larger times.

4.2. Two-Layer Shallow Water Equations

In this section, we proceed with three numerical examples for the two-layer shallow water equations (1), (16). We take $r = 0.98$ and either $g = 10$ (Examples 3 and 5) or $g = 1$ (Example 4).

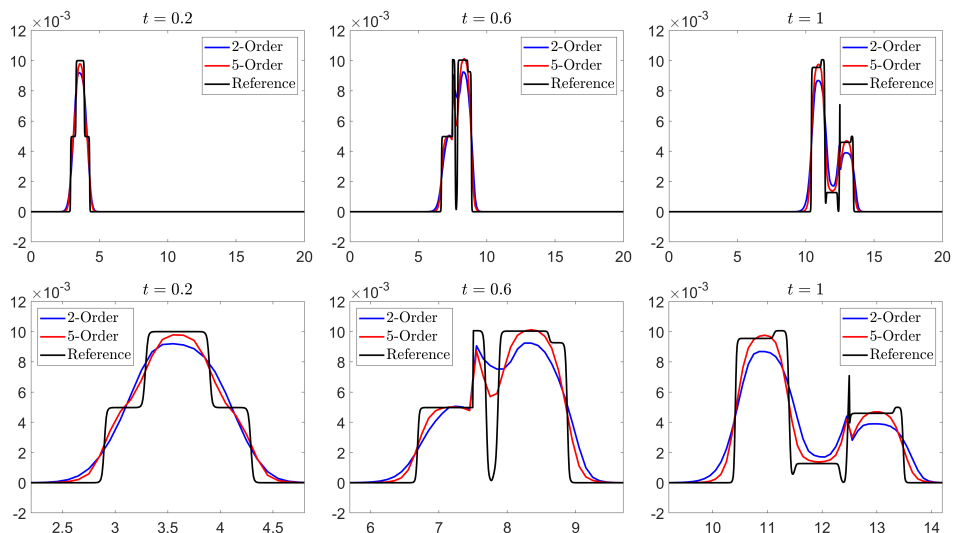


Figure 3: Example 2: The difference $\rho(x, t) - \rho_{eq}$ (top row) and zoom at the perturbations (bottom row) at times $t = 0.2$ (left column), 0.6 (middle column), and 1 (right column).

Example 3—Experimental Order of Accuracy. In this example taken from [25], we consider the following initial data:

$$\begin{aligned} h_1(x, 0) &= 5 + e^{\cos(2\pi x)}, & h_2(x, 0) &= 5 - e^{\cos(2\pi x)} - \sin^2(\pi x), \\ q_1(x, 0) &= q_2(x, 0) \equiv 0, \end{aligned}$$

and a continuous bottom topography

$$Z(x) = \sin^2(\pi x) - 10,$$

both prescribed in the computational domain $[0, 1]$ subject to the periodic boundary conditions.

We compute the numerical solution until the final time $t = 0.1$ by both the 2-Order and 5-Order Schemes on a sequence of uniform meshes with $\Delta x = 1/40, 1/80, 1/160, 1/320, 1/640,$ and $1/1280$. We measure the L^1 -errors in h_1 and estimate the experimental convergence rates using the following Runge formulae, which are based on the solutions computed on the three consecutive uniform grids with the mesh sizes $\Delta x, 2\Delta x,$ and $4\Delta x$ and

denoted by $(\cdot)^{\Delta x}$, $(\cdot)^{2\Delta x}$, and $(\cdot)^{4\Delta x}$, respectively:

$$\text{Error}(\Delta x) \approx \frac{\delta_{12}^2}{|\delta_{12} - \delta_{24}|}, \quad \text{Rate}(\Delta x) \approx \log_2 \left(\frac{\delta_{24}}{\delta_{12}} \right).$$

Here, $\delta_{12} := \|(\cdot)^{\Delta x} - (\cdot)^{2\Delta x}\|_{L^1}$ and $\delta_{24} := \|(\cdot)^{2\Delta x} - (\cdot)^{4\Delta x}\|_{L^1}$. The obtained results for the density are reported in Table 1, where one can clearly see that the expected orders of accuracy are achieved by both the 2-Order and 5-Order Schemes. Note that in order to achieve the fifth order of accuracy, we have used smaller time steps with $\Delta t \sim (\Delta x)^{\frac{5}{3}}$.

Table 1: Example 3: The L^1 -errors and experimental convergence rates for h_1 .

Δx	2-Order		5-Order	
	Error	Rate	Error	Rate
1/160	5.64e-4	2.58	1.90e-7	4.83
1/320	6.18e-5	2.86	5.10e-9	5.02
1/640	1.38e-5	2.54	1.57e-10	5.02
1/1280	1.75e-6	2.74	4.86e-12	5.01

Example 4—Small Perturbation of Discontinuous Steady State.

In this example, we consider a discontinuous steady state given by

$$\begin{aligned} (h_1)_{\text{eq}}(x) &:= \begin{cases} 1.22373355048230, & x < 0, \\ 1.44970064153589, & x > 0, \end{cases} & (q_1)_{\text{eq}}(x) &\equiv 12, \\ (h_2)_{\text{eq}}(x) &:= \begin{cases} 0.968329515483846, & x < 0, \\ 1.12439026921484, & x > 0, \end{cases} & (q_2)_{\text{eq}}(x) &\equiv 10, \end{aligned} \quad (20)$$

and a discontinuous bottom topography

$$Z(x) = \begin{cases} -2, & x < 0, \\ -1, & x > 0. \end{cases} \quad (21)$$

In order to demonstrate that the proposed 2-Order and 5-Order Schemes are WB, we use (20)–(21) as the initial setting prescribed in the computational domain $[-1, 1]$ subject to free boundary conditions and compute the numerical solution until the final time $t = 20$ on a uniform mesh with $\Delta x = 1/100$. The obtained discrete L^1 - and L^∞ -errors are reported in Table

Table 2: Example 4: L^1 -errors for h_1 , h_2 , q_1 , and q_2 .

	L^1 -error in h_1	L^1 -error in h_2	L^1 -error in q_1	L^1 -error in q_2
2-Order	1.77e-17	2.58e-17	1.42e-16	2.13e-16
5-Order	4.44e-17	3.37e-16	1.40e-15	4.96e-15

2, where one can clearly see that both the 2-Order and 5-Order Schemes can preserve the steady state within the machine accuracy.

We then test the ability of the studied 2-Order and 5-Order Schemes to capture small perturbations of this steady state, which is initially added to the upper layer depth:

$$h_1(x, 0) = (h_1)_{\text{eq}}(x) + \begin{cases} 0.001, & x \in [-0.6, -0.5], \\ 0, & \text{otherwise,} \end{cases}$$

$$h_2(x, 0) = (h_2)_{\text{eq}}(x), \quad q_1(x, 0) = (q_1)_{\text{eq}}(x), \quad q_2(x, 0) = (q_2)_{\text{eq}}(x).$$

We compute the numerical solution until the final time $t = 0.08$ by both the 2-Order and 5-Order Schemes on a uniform mesh with $\Delta x = 1/100$ and plot the difference $h_1(x, t) - (h_1)_{\text{eq}}(x)$ at times $t = 0.02, 0.05$, and 0.08 in Figure 4. Here, the reference solution is computed by the 5-Order Scheme on a much finer mesh with $\Delta x = 1/5000$. As one can see, the 5-Order Scheme outperforms the 2-Order Scheme.

Example 5—Convergence to a Moving-Water Steady State. In the fourth example, we first demonstrate the ability of the proposed 5-Order Scheme to reach discrete steady state. To this end, we take constant initial data

$$h_1(x, 0) \equiv 8, \quad h_2(x, 0) \equiv 4, \quad q_1(x, 0) = q_2(x, 0) \equiv 0,$$

and a discontinuous bottom topography

$$Z(x) = \begin{cases} 0.2, & x \in [8, 12], \\ 0, & \text{otherwise,} \end{cases}$$

both prescribed in the computational domain $[0, 25]$ subject to the Dirichlet boundary conditions imposed at $x = 0$,

$$h_1(0, t) = 8, \quad (h_2)(0, t) = 4, \quad (q_1)(0, t) = 119, \quad (q_2)(0, t) = 60,$$

and free boundary conditions imposed at $x = 25$.

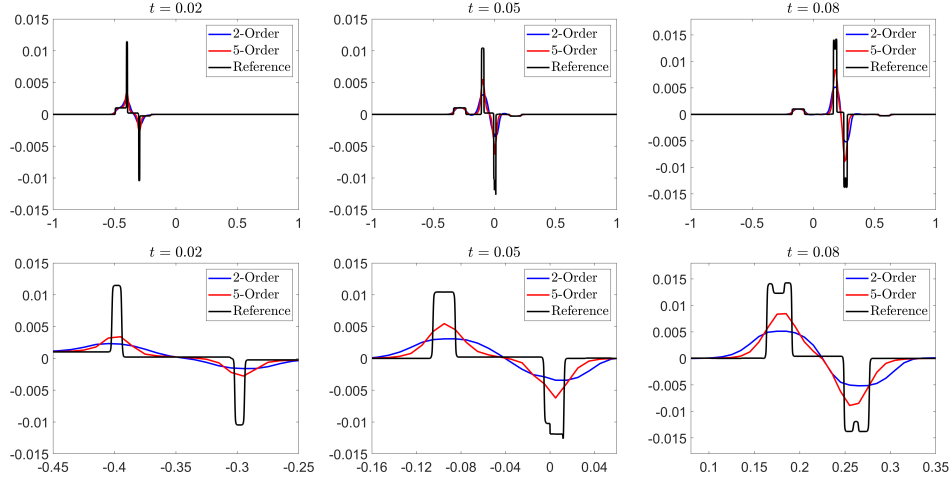


Figure 4: Example 4: The difference $h_1(x, t) - (h_1)_{\text{eq}}$ (top row) and zoom at the perturbations (bottom row) at times $t = 0.02$ (left column), 0.05 (middle column), and 0.08 (right column).

We first compute the numerical solutions on a uniform mesh with $\Delta x = 1/5$ until a very large time $t = 100$ to let the solution to converge to the discrete steady state. The obtained results agree almost perfectly with those reported in [23, Figure 7.20] for the 2-Order Scheme.

We then add a small perturbation to the upper layer water depth and consider the following initial data:

$$h_1(x, 0) = (h_1)_{\text{eq}}(x) + \begin{cases} 0.0001, & x \in [2, 2.25], \\ 0, & \text{otherwise,} \end{cases}$$

$$h_2(x, 0) = (h_2)_{\text{eq}}(x), \quad q_1(x, 0) = (q_1)_{\text{eq}}(x), \quad q_2(x, 0) = (q_2)_{\text{eq}}(x),$$

subject to free boundary conditions at both ends of the computational domain.

We compute the numerical solutions until the final time $t = 1$ by both the 2-Order and 5-Order Schemes on a uniform mesh with $\Delta x = 1/5$. The obtained differences $h_1 - (h_1)_{\text{eq}}$ at times $t = 0.2, 0.6,$ and 1 are plotted in Figure 5 together with the reference solution computed by the 5-Order Scheme on a finer mesh with $\Delta x = 1/20$. One can observe that the 5-Order Scheme produces sharper results compared to those obtained by the 2-Order Scheme.

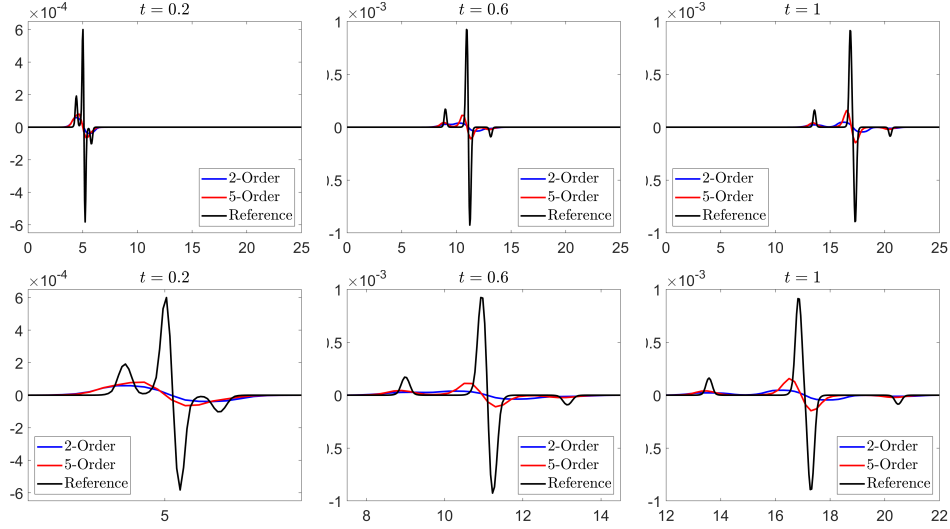


Figure 5: Example 5: The difference $h_1(x, t) - (h_1)_{\text{eq}}$ (top row) and zoom at the perturbations (bottom row) at times $t = 0.2$ (left column), 0.6 (middle column), and 1 (right column).

Example 6—Riemann Problems. In the final example, we numerically solve two Riemann problems with the following initial data:

$$\begin{aligned} \text{Test1 : } (h_1, q_1, h_2, q_2)(x, 0) &= \begin{cases} (1, 1.5, 1, 1), & x < 0, \\ (0.8, 1.2, 1.2, 1.8), & \text{otherwise,} \end{cases} \\ \text{Test2 : } (h_1, q_1, h_2, q_2)(x, 0) &= \begin{cases} (1.5, 1, 1, 1.5), & x < 0, \\ (1.2, 1.6, 0.9, 1.2), & \text{otherwise,} \end{cases} \end{aligned}$$

with a discontinuous bottom topography,

$$Z(x) = \begin{cases} -2, & x < 0, \\ -1.5, & \text{otherwise,} \end{cases}$$

prescribed in the computational domain $[-1, 1]$ subject to free boundary conditions.

The numerical solutions computed by the 2-Order and 5-Order Schemes until time $t = 0.1$ on a uniform mesh with $\Delta x = 1/50$ are plotted in Figures 6 and 7 together with the reference solution computed by the 5-Order Scheme on a much finer mesh with $\Delta x = 1/2000$. As one can see, the results obtained

by the 5-Order Scheme are sharper and less oscillatory compared to those computed by the 2-Order Scheme.

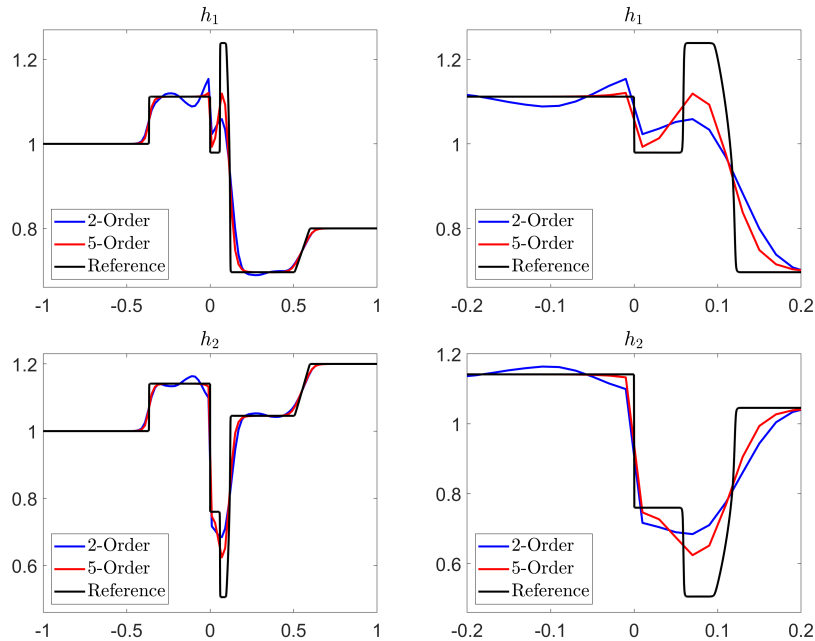


Figure 6: Example 6 (Test 1): h_1 and h_2 (left column) and zoom at $x \in [-0.2, 0.2]$ (right column).

5. Conclusions

In this paper, we have extended the second-order finite-volume flux globalization based well-balanced (WB) path-conservative central-upwind (PCCU) schemes to fifth order of accuracy via the framework of the finite-difference alternative weighted essentially non-oscillatory (A-WENO) schemes. The developed fifth-order flux globalization based WB A-WENO PCCU schemes have been applied to two nonconservative systems—the nozzle flow system and two-layer shallow water equations. We have tested the fifth-order schemes on a number of numerical examples and demonstrated that they clearly outperform their second-order counterparts.

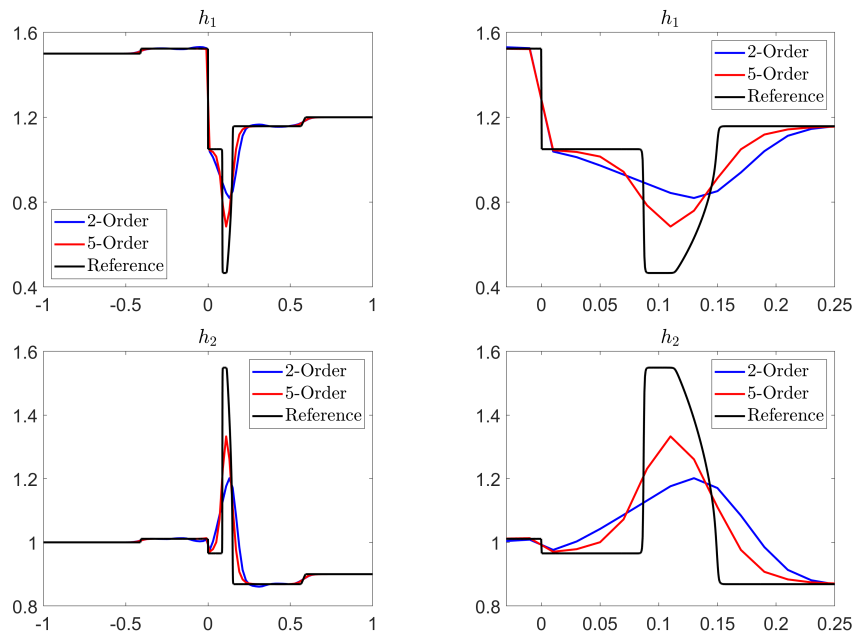


Figure 7: Example 6 (Test 2): h_1 and h_2 (left column) and zoom at $x \in [-0.03, 0.25]$ (right column).

Acknowledgements

The work of S. Chu was supported in part by the DFG (German Research Foundation) through HE5386/19-3, 27-1. The work of A. Kurganov was supported in part by NSFC grant 12171226 and by the fund of the Guangdong Provincial Key Laboratory of Computational Science and Material Design (No. 2019B030301001).

References

- [1] S. Busto, M. Dumbser, S. Gavrilyuk and K. Ivanova, On thermodynamically compatible finite volume methods and path-conservative ADER discontinuous Galerkin schemes for turbulent shallow water flows. *J. Sci. Comput.* **88** (2021), Paper No. 28, 45 pp. [MR4274288](#)
- [2] Y. Cao, A. Kurganov and Y. Liu, Flux globalization based well-balanced path-conservative central-upwind scheme for the thermal rotating shallow water equations. *Commun. Comput. Phys.* **34** (2023), 993–1042. [MR4668444](#)

- [3] Y. Cao, A. Kurganov, Y. Liu and R. Xin, Flux globalization based well-balanced path-conservative central-upwind schemes for shallow water models. *J. Sci. Comput.* **92** (2022), Paper No. 69, 31 pp. [MR4450104](#)
- [4] Y. Cao, A. Kurganov, Y. Liu and V. Zeitlin, Flux globalization based well-balanced path-conservative central-upwind scheme for two-layer thermal rotating shallow water equations. *J. Comput. Phys.* **474** (2023), Paper No. 111790, 29 pp. [MR4515239](#)
- [5] V. Caselles, R. Donat and G. Haro, Flux-gradient and source-term balancing for certain high resolution shock-capturing schemes. *Comput. & Fluids* **38** (2009), 16–36. [MR2645613](#)
- [6] M. J. Castro, T. Morales de Luna and C. Parés, Well-balanced schemes and path-conservative numerical methods, in Handbook of numerical methods for hyperbolic problems, vol. 18 of Handb. Numer. Anal. Elsevier/North-Holland, Amsterdam (2017), 131–175. [MR3645391](#)
- [7] C. Chalons, Path-conservative in-cell discontinuous reconstruction schemes for non conservative hyperbolic systems. *Commun. Math. Sci.* **18** (2020), 1–30. [MR4084141](#)
- [8] M. J. Castro Díaz, A. Kurganov and T. Morales de Luna, Path-conservative central-upwind schemes for nonconservative hyperbolic systems. *ESAIM Math. Model. Numer. Anal.* **53** (2019), 959–985. [MR3969161](#)
- [9] Y. Chen, A. Kurganov and M. Na, A Flux Globalization Based Well-Balanced Path-Conservative Central-Upwind Scheme for the Shallow Water Flows in Channels. *ESAIM Math. Model. Numer. Anal.* **57** (2023), 1087–1110. [MR4574005](#)
- [10] A. Chertock, S. Chu and A. Kurganov, Adaptive high-order A-WENO schemes based on a new local smoothness indicator. *E. Asian. J. Appl. Math.* **13** (2023), 576–609. [MR4600448](#)
- [11] A. Chertock, M. Herty and Ş. N. Özcan, Well-balanced central-upwind schemes for 2×2 systems of balance laws, in Theory, Numerics and Applications of Hyperbolic Problems. I, vol. 236 of Springer Proc. Math. Stat. Springer, Cham (2018), 345–361. [MR3828226](#)
- [12] S. Chu, A. Kurganov and S. Mohammadian and Z. Zheng, Fifth-order A-WENO path-conservative central-upwind scheme for behavioral non-equilibrium traffic models. *Commun. Comput. Phys.* **33** (2023), 692–732. [MR4598246](#)

- [13] S. Chu, A. Kurganov and M. Na, Fifth-order A-WENO schemes based on the path-conservative central-upwind method. *J. Comput. Phys.* **469** (2022), Paper No. 111508, 22 pp. [MR4471537](#)
- [14] S. Chu, A. Kurganov and R. Xin, New more efficient A-WENO schemes. Preprint available at <https://sites.google.com/view/alexander-kurganov/publications>.
- [15] G. Dal Maso, P. G. Lefloch and F. Murat, Definition and weak stability of nonconservative products. *J. Math. Pures Appl.* **74** (1995), 483–548. [MR1365258](#)
- [16] W. S. Don, R. Li, B.-S. Wang and Y. H. Wang, A novel and robust scale-invariant WENO scheme for hyperbolic conservation laws. *J. Comput. Phys.* **448** (2022), Paper No. 110724, 23 pp. [MR4319348](#)
- [17] D. Donat and A. Martinez-Gavara, Hybrid second order schemes for scalar balance laws. *J. Sci. Comput.* **48** (2011), 52–69. [MR2811690](#)
- [18] L. Gascón and J. M. Corderán, Construction of second-order TVD schemes for nonhomogeneous hyperbolic conservation laws. *J. Comput. Phys.* **172** (2001), 261–297. [MR1852329](#)
- [19] S. Gottlieb, D. Ketcheson and C.-W. Shu, Strong stability preserving Runge-Kutta and multistep time discretizations. World Scientific Publishing Co. Pte. Ltd., Hackensack, NJ (2011). [MR2789749](#)
- [20] S. Gottlieb, C.-W. Shu and E. Tadmor, Strong stability-preserving high-order time discretization methods. *SIAM Rev.* **43** (2001), 89–112. [MR1854647](#)
- [21] Y. Jiang, C.-W. Shu and M. Zhang, An alternative formulation of finite difference weighted ENO schemes with Lax-Wendroff time discretization for conservation laws. *SIAM J. Sci. Comput.* **35** (2013), A1137–A1160. [MR3045660](#)
- [22] A. Kurganov and C.-T. Lin, On the reduction of numerical dissipation in central-upwind schemes. *Commun. Comput. Phys.* **2** (2007), 141–163. [MR2305919](#)
- [23] A. Kurganov, Y. Liu and R. Xin, Well-Balanced Path-Conservative Central-Upwind Schemes Based on Flux Globalization. *J. Comput. Phys.* **474** (2023), Paper No. 111773, 32 pp. [MR4513801](#)
- [24] A. Kurganov, S. Noelle and G. Petrova, Semi-discrete central-upwind schemes for hyperbolic conservation laws and Hamilton-Jacobi equations. *SIAM J. Sci. Comput.* **23** (2001), 707–740. [MR1860961](#)

- [25] A. Kurganov and G. Petrova, Central-upwind schemes for two-layer shallow water equations. *SIAM J. Sci. Comput.* **31** (2009), 1742–1773. [MR2491544](#)
- [26] A. Kurganov and E. Tadmor, New high-resolution central schemes for nonlinear conservation laws and convection-diffusion equations. *J. Comput. Phys.* **160** (2000), 241–282. [MR1756766](#)
- [27] P. G. LeFloch, Hyperbolic systems of conservation laws, Lectures in Mathematics ETH Zürich, Birkhäuser Verlag, Basel (2002). The theory of classical and nonclassical shock waves. [MR1927887](#)
- [28] P. G. LeFloch, Graph solutions of nonlinear hyperbolic systems. *J. Hyperbolic Differ. Equ.* **1** (2004), 643–689. [MR2111578](#)
- [29] P. Li, T. T. Li, W. S. Don and B.-S. Wang, Scale-invariant multi-resolution alternative WENO scheme for the Euler equations. *J. Sci. Comput.* **94** (2023), Paper No. 15, 32 pp. [MR4519622](#)
- [30] K.-A. Lie and S. Noelle, On the artificial compression method for second-order nonoscillatory central difference schemes for systems of conservation laws. *SIAM J. Sci. Comput.* **24** (2003), 1157–1174. [MR1976211](#)
- [31] H. Liu, A numerical study of the performance of alternative weighted ENO methods based on various numerical fluxes for conservation law. *Appl. Math. Comput.* **296** (2017), 182–197. [MR3572788](#)
- [32] A. Martinez-Gavara and R. Donat, A hybrid second order scheme for shallow water flows. *J. Sci. Comput.* **48** (2011), 241–257. [MR2811701](#)
- [33] H. Nessyahu and E. Tadmor, Nonoscillatory central differencing for hyperbolic conservation laws. *J. Comput. Phys.* **87** (1990), 408–463. [MR1047564](#)
- [34] C. Parés, Path-conservative numerical methods for nonconservative hyperbolic systems, in Numerical methods for balance laws, vol. 24 of Quad. Mat., Dept. Math., Seconda Univ. Napoli, Caserta (2009), 67–121. [MR2976968](#)
- [35] E. Pimentel-García, M. J. Castro, C. Chalons, T. Morales de Luna and C. Parés, In-cell discontinuous reconstruction path-conservative methods for non conservative hyperbolic systems—second-order extension. *J. Comput. Phys.* **459** (2022), Paper No. 111152, 35 pp. [MR4401970](#)
- [36] K. A. Schneider, J. M. Gallardo, D. S. Balsara, B. Nkonga and C. Parés, Multidimensional approximate Riemann solvers for hyperbolic noncon-

- servative systems. Applications to shallow water systems. *J. Comput. Phys.* **444** (2021), Paper No. 110547, 49 pp. [MR4287467](#)
- [37] C.-W. Shu, High order weighted essentially nonoscillatory schemes for convection dominated problems. *SIAM Rev.* **51** (2009), 82–126. [MR2481112](#)
- [38] C.-W. Shu, Essentially non-oscillatory and weighted essentially non-oscillatory schemes. *Acta Numer.* **29** (2020), 701–762. [MR4189296](#)
- [39] P. K. Sweby, High resolution schemes using flux limiters for hyperbolic conservation laws. *SIAM J. Numer. Anal.* **21** (1984), 995–1011. [MR0760628](#)
- [40] B.-S. Wang and W. S. Don, Affine-invariant WENO weights and operator. *Appl. Numer. Math.* **181** (2022), 630–646. [MR4457761](#)
- [41] B.-S. Wang, W. S. Don, N. K. Garg and A. Kurganov, Fifth-order A-WENO finite-difference schemes based on a new adaptive diffusion central numerical flux. *SIAM J. Sci. Comput.* **42** (2022), A3932–A3956. [MR4186540](#)
- [42] B.-S. Wang, W. S. Don, A. Kurganov and Y. Liu, Fifth-order A-WENO schemes based on the adaptive diffusion central-upwind Rankine-Hugoniot fluxes. *Commun. Appl. Math. Comput.* **5** (2023), 295–314. [MR4547999](#)
- [43] B.-S. Wang, P. Li, Z. Gao and W. S. Don, An improved fifth order alternative WENO-Z finite difference scheme for hyperbolic conservation laws. *J. Comput. Phys.* **374** (2018), 469–477. [MR3864459](#)

SHAOSHUAI CHU

DEPARTMENT OF MATHEMATICS, RWTH AACHEN UNIVERSITY, AACHEN,
52056

GERMANY

E-mail address: chuss2019@mail.sustech.edu.cn

ALEXANDER KURGANOV

DEPARTMENT OF MATHEMATICS, SHENZHEN INTERNATIONAL CENTER FOR
MATHEMATICS, AND GUANGDONG PROVINCIAL KEY LABORATORY OF
COMPUTATIONAL SCIENCE AND MATERIAL DESIGN, SOUTHERN UNIVERSITY OF
SCIENCE AND TECHNOLOGY, SHENZHEN, 518055

CHINA

E-mail address: alexander@sustech.edu.cn

RUIXIAO XIN

DEPARTMENT OF MATHEMATICS, SOUTHERN UNIVERSITY OF SCIENCE AND
TECHNOLOGY, SHENZHEN, 518055
CHINA

E-mail address: 12331009@mail.sustech.edu.cn

RECEIVED 1 JANUARY 2024